International Journal of Multiphysics
Volume 18, No. 2s, 2024
ISSN: 1750-9548

Modelling Convection-Diffusion Phenomena by Direct and Indirect Meshless Methods

K Chanthawara[1], P Paewpolsong[2], D Ritthison[2], S Kaennakham[2*]

[1.] Program of Mathematics, Faculty of Science, Ubon Ratchathani Rajabhat University, Ubon Ratchathani, 34000, Thailand

[2.] School of Mathematics, Institute of Science, Suranaree University of Technology, Nakhon Ratchasima, 30000, Thailand

*Corresponding author sayan_kk@g.sut.ac.th

Abstract

Time-dependent convection-diffusion problems, prevalent in science and engineering, present significant analytical challenges. The limitations of traditional mesh-based numerical methods necessitate alternative approaches. Meshless methods emerge as a pivotal solution, offering precision where conventional techniques falter. This research centers on applying meshless methods to such problems, emphasizing their critical role in accurately modelling complex phenomena across various applications. Methodologically, the research compares two specific meshless methods: the Direct method and the Indirect method. Both methods are implemented using the multiquadric radial basis function within a global collocation framework. The Direct method is derivative-based, while Indirect adopts an integration-based approach. The comparison is conducted over four different test cases, which are designed to assess the sensitivity of Direct and Indirect to the multiquadric shape parameter and node density, their effectiveness under varying convection forces, and their computational efficiency.The findings of the study are twofold. Firstly, the Direct method exhibits superior accuracy overall, particularly in scenarios with intense convection and in capturing boundary layers characterized by steep flow variable gradients. Secondly, the Indirect method demonstrates notable computational efficiency, requiring approximately half the computational time needed by the Direct method. However, this efficiency comes with a trade-off in accuracy, particularly under conditions of high convection. The research concludes that the choice between the Direct and Indirect methods should be based on the specific demands of the problem, considering factors such as the desired level of accuracy, available computational resources, and the complexity of the scenario. This study offers valuable insights for professionals in fields like environmental science and pollution control, aiding in the selection of the most suitable meshless method for effectively tackling convection-diffusion challenges.

1. INTRODUCTION

Real-world problems have often time become possible for human to tackle when they are modelled or represented by Partial Differential Equations (PDEs). With this, PDEs play crucial roles in many areas of applications in science, engineering, physics, chemistry, ecology, biology, and many more [1-5]. There are different types of PDEs; linear or nonlinear; homogeneous or nonhomogeneous; elliptic, hyperbolic, or parabolic, each of which holds different mathematical characteristics and represents different physical phenomenon. Convection-diffusion equations are specific forms of PDEs and have been attracting an increasing amount of attention [6-9]. They are found to play a significant role in various fields of science, engineering, and ecosystem including (as models for)

air pollution [10], adsorption of pollutants in soil, food processing [11], fluid flows, climate studies, astrophysics [12], groundwater prediction and environmental protection [13] (refer to the references cited therein), energy [14], financial-related issues [15], and various branches of mathematics related to pattern formation [12]. As long as the ecosystem is concerned, in particular, by understanding the movement and distribution of substances within ecosystems, we can make informed decisions to promote sustainable development, protect biodiversity, and ensure the long-term health and resilience of ecosystems. Investing in accurate prediction of convection-diffusion phenomena is crucial for achieving environmental sustainability and preserving the intricate web of life on our planet. With this huge impact in these many areas, finding solutions for them has inevitably become necessary. Like other kinds of PDEs, there are two main types of solution: analytical and numerical. While it is well-known that analytical solutions are extremely difficult to achieve (or even not at all possible, particularly for complex problems), in this work, the main focus is on the numerical side of solution finding strategies.

Over decades, the conventional and standard numerical methods for solving the convection-diffusion equation are finite different method (FDM) [16-18], finite element method (FEM) [19] [20], and finite volume method (FVM) [21, 22]. The most challenging issue under this kind of phenomena is the oscillatory occurring. For this crucial task, the forementioned conventional schemes are often supported with some special numerical treatments such as the stabilized methods [10, 23], the up-winding schemes and adding a consistent diffusion term in streamline direction known as the streamline upwind Petrov–Galerkin method [24], the local projection stabilization method [25], the stencil finite-different method [26]. Another promising extra treatment may be to get help from additional grids/mesh known as ‘grid/mesh refinement’ where denser grids are expected to take place at locations with high gradient of problem variables such as boundary layers. This, however, comes with a high price to pay in terms of CPU time and space as refining grids/mesh is a highly complex process. A nicely documented work recently done along this path is [27] (see also references therein).

To avoid complexities arising with grid/mesh-based methods, numerical schemes constructed with aims to be independent of grid/mesh as much as possible have been receiving a great amount of attention during the past decades. Numerical studies under this concept include the use of the boundary element method [28-31], and those known as ‘meshfree/meshless’ methods. Meshless methods have been widely applied to the solution of PDEs [32, 33]. Compared with the traditional numerical methods, meshless methods do not need grid/mesh generation and they have been proven to be capable of tackling complex problems in high dimensions. Generally, this family of methods can be grouped into two classes; (i) strong forms including radial basis function collocation methods [34], the finite point method [35], the hp-meshless cloud method [36], etc., (ii) weak forms including the element free Galerkin method [37], the diffuse element method [38], and the point interpolation method [39], etc., and see references therein. Those based on radial basis functions (RBFs) are what the main attention of this work is paid to.

The radial basis function of multiquadric type was firstly numerically explored in a global manner for the context of interpolation and, later for solving PDEs by Kansa in 1990 [40]. Ever since, a vast number of applications have been growing in many branches of science and engineering [41, 42]. Some recent works (only over the past decade) include the examination of evaluation algorithm [43], the solution to seepage problems using a new algorithm for the shape parameter optimization [44], the determination of the optimal shape parameter in the multiquadric function [45], the solution to time-fractional higher order partial differential equations with constant and variable coefficients [46], and the computational study on constant and sinusoidal heating of skin tissue [47]. With regards to solving convection-diffusion type of PDEs, recent numerical works based on RBFs include the H -adaptive RBF-FD method for the high-dimensional equations [48], the RBF-FD method based on Shishkin nodes [49], the comparative investigation on RBF shape parameters [50], the attempt to improve the results quality by the means of automatic node-adaptation [51-53], and the comparative study of four internal-node-free schemes [54].

In this work, it focuses on an application of RBF when being used as a component of a differential quadrature (DQ) numerical scheme. The idea to replace the polynomial term appearing in the original DQ, proposed in 1972 by Bellman [55], was firstly done by Wu and Shu in 2002 [56] where the main focus was paid on the approximation of the derivative terms (referred hereafter in this work as ‘Direct (DR)’ method). Recent successful

studies of the method are the application for elliptic problems in axisymmetric domain [57], for time-dependent analysis of unsaturated seepage [58], and for solving non-linear differential equations of Lane-Emden type [59] (see also the references therein). Alternatively, for the sake of comparison, the attempt to make use of the integration of RBF firstly proposed by Mai Duy in 2005 [60] is also under investigation in this work (referred hereafter in this work as 'Indirect (iDR)' method). This method was later investigated in more comprehensive detail by Sarra in 2006 [61] where the most recent researches include the applications for the second-order differential problems [62], the natural convection in concentric annuli [63], and the numerical simulation of shallow water waves based on generalized equal width (GEW) equation [64], to name only a few.

Section 2 of the paper provides the mathematical idea and structure of both DR and iDR methods before their implementation to the time-dependent convection-diffusion is described in Section 3. Section 4 gives the numerical algorithm where four numerical examples are demonstrated in Section 5 and the main conclusions are drawn in Section 6.

2. MATHEMATICAL BLACKGROUND

2.1. The RBF- differential quadrature (direct, DR) method

The original radial basis function-differential quadrature (RBF-DQ) method states that a weighted linear sum of the functional values at neighboring nodes can approximate the derivatives of a smooth function. Since only two-dimensional problems are considered, it is defined that $\mathbf{p}_i = (x_i, y_i)$ denotes the *i*th node. The implies that at the *i*th node $\mathbf{p}_i$, the RBF-DQ approximation for the *n*-th order derivative of $u(\mathbf{p})$ with respect to, $\xi = \{x, y\}$, can be stated as $u_\xi^{(n)}$

$$u_\xi^{(n)}(\mathbf{p}_i) = \sum_{j=1}^{N} w_{ij}^{(n,\xi)} u(\mathbf{p}_j), \tag{1}$$

where $w_{ij}^{(n,\xi)}$ are the DQ weighting coefficients, and N is the total number of nodes used in the supporting region. For a global scheme, like studied in this work, this N implies the number of nodes in the entire computational domain.

It is assumed that there are N nodes, $\mathbf{p}_1, \mathbf{p}_2, ..., \mathbf{p}_N$, in the support domain of point $\mathbf{p}$ in the standard RBF-DQ technique procedure. Then, the RBFs' approximation of u can be expressed as

$$u(\mathbf{p}) = \sum_{k=1}^{N} \lambda_k \varphi_k(\mathbf{p}), \tag{2}$$

where λ_k is the coefficient for a selected radial basis function, $\varphi_k(\mathbf{p})$. In this work, a popular choice of RBFs known as 'multiquadric (MQ)' is under investigation and its formula is expressed as follows

$$\varphi_k(\mathbf{p}) = \sqrt{r_k^2 + c^2}, \tag{3}$$

where the positive constant c is known as the shape parameter and it is this parameter that is known to play a crucial role in solution quality determination, and r_k is the distance between point $\mathbf{p}$ and $\mathbf{p}_k$, generally taken to be the Euclidean format, i.e.,

$$r_k = \|\mathbf{p} - \mathbf{p}_k\|. \tag{4}$$

Equation (2) can be used to build an N-dimensional linear vector space V_N because it has N freedoms. In Equation (2), $\{\varphi_k(\mathbf{p}), k = 1, 2, ..., N\}$ is a set of basis functions in V_N that can be regarded as the basis vectors. The

weighting coefficients $w_{ij}^{(n,\xi)}$ can, therefore, be calculated in the same manner as the conventional DQ technique. Equation (1) yields the following when all basis functions are substituted:

$$\frac{\partial^{(n)}\varphi_k\left(\mathbf{p}_i\right)}{\partial\xi^{(n)}}=\sum_{j=1}^{N}w_{ij}^{(n,\xi)}\varphi_k\left(\mathbf{p}_j\right). \tag{5}$$

It can be expressed in a clearer format as follows

$$\underbrace{\begin{bmatrix}\frac{\partial^{(n)}\varphi_1\left(\mathbf{p}_i\right)}{\partial\xi^{(n)}}\\ \frac{\partial^{(n)}\varphi_2\left(\mathbf{p}_i\right)}{\partial\xi^{(n)}}\\ \vdots\\ \frac{\partial^{(n)}\varphi_N\left(\mathbf{p}_i\right)}{\partial\xi^{(n)}}\end{bmatrix}}_{\frac{\partial^{(n)}\vec{\varphi}(\mathbf{p}_i)}{\partial\xi^{(n)}}}=\underbrace{\begin{bmatrix}\varphi_1\left(\mathbf{p}_1\right) & \varphi_1\left(\mathbf{p}_2\right) & \cdots & \varphi_1\left(\mathbf{p}_N\right)\\ \varphi_2\left(\mathbf{p}_1\right) & \varphi_2\left(\mathbf{p}_2\right) & \cdots & \varphi_2\left(\mathbf{p}_N\right)\\ & & \ddots & \\ \varphi_N\left(\mathbf{p}_1\right) & \varphi_N\left(\mathbf{p}_2\right) & \cdots & \varphi_N\left(\mathbf{p}_N\right)\end{bmatrix}}_{[A]}\underbrace{\begin{bmatrix}w_{i1}^{(n,\xi)}\\ w_{i2}^{(n,\xi)}\\ \vdots\\ w_{iN}^{(n,\xi)}\end{bmatrix}}_{\vec{w}_i^{(n,\xi)}}. \tag{6}$$

It is to be noted that since we apply direct differentiations to φ on the left-hand side of Equation (6), this procedure, is referred to hereafter as the "Direct method (DR)". The matrix $[A]$ is invertible if the appropriate φ is selected, in accordance with the theory of RBF approximation. Consequently, the following equation can be used to find the vector $w_i^{(n,\xi)}$,

$$\vec{w}_i^{(n,\xi)}=[A]^{-1}\frac{\partial^{(n)}\vec{\varphi}\left(\mathbf{p}_i\right)}{\partial\xi^{(n)}},\quad i=1,2,...,N. \tag{7}$$

This resulting vector from Equation (7) is not to be input into Equation (1) and the following can be achieved for the derivative of u,

$$u_{\xi}^{(n)}\left(\mathbf{p}_i\right)=\sum_{j=1}^{N}w_{ij}^{(n,\xi)}u\left(\mathbf{p}_j\right). \tag{8}$$

2.2. The integrated RBF- differential quadrature (indirect, iDR) method

In contrast with the direct method described above, in the integrated RBF-DQ (iRBF-DQ) start with the approximation of the highest order of derivative occurring in the governing equation. This means that for a second-order derivative $u''\left(\mathbf{p}\right)$, its approximation can be defined under this concept as

$$u_x^{(2)}\left(\mathbf{p}\right)=\sum_{k=1}^{N}\mu_k\varphi_k\left(\mathbf{p}\right). \tag{9}$$

From this point, an integration procedure, with respect to x can be performed.

$$\begin{aligned} u_x^{(1)}(\mathbf{p}) &= \int u_x^{(2)}(\mathbf{p})dx = \int \sum_{k=1}^{N} \mu_k \varphi_k(\mathbf{p})dx \\ &= \sum_{k=1}^{N} \mu_k \int \varphi_k(\mathbf{p})dx \\ &= \sum_{k=1}^{N} \mu_k H_k(\mathbf{p}) + C_2(y). \end{aligned} \tag{10}$$

The same procedure is again repeated to yield the following

$$\begin{aligned} u(\mathbf{p}) &= \int u_x^{(1)}(\mathbf{p})dx = \int \left(\sum_{k=1}^{N} \mu_k H_k(\mathbf{p}) + C_2(y) \right) dx \\ &= \sum_{k=1}^{N} \mu_k \int H_k(\mathbf{p})dx + C_2(y)x + C_1(y) \\ &= \sum_{k=1}^{N} \mu_k \bar{H}_k(\mathbf{p}) + C_2(y)x + C_1(y), \end{aligned} \tag{11}$$

where $H_k(\mathbf{p}) = \int \varphi_k(\mathbf{p})dx$, $\bar{H}_k(\mathbf{p}) = \int H_k(\mathbf{p})dx$ and μ_k are their coefficients. Note that integration with respect to y can be done similarly. The additional polynomial term in both Equation (10) and Equation (11) can be achieved by minimizing the sum of squared errors as nicely done in [65]. Nevertheless, we have observed from the work of [63] that the method can still perform well even without the polynomial term so it is omitted in this work.

As previously stated, only the multiquadric MQ-RBF is considered and according to Shu and Wu [63], the expressions for the integrated MQ-RBF can be expressed as follows

$$\begin{aligned} H_k^{(\xi)}(\mathbf{p}) &= \int \varphi_k(\mathbf{p})d\xi \\ &= \frac{\left(\xi_{\mathbf{p}} - \xi_{\mathbf{p}_k}\right)\sqrt{r_k^2 + c^2}}{2} + \frac{r_k^2 - \left(\xi_{\mathbf{p}} - \xi_{\mathbf{p}_k}\right)^2 + c^2}{2} \ln\left(\xi_{\mathbf{p}} - \xi_{\mathbf{p}_k} + \sqrt{r_k^2 + c^2}\right), \end{aligned} \tag{12}$$

$$\begin{aligned} \bar{H}_k^{(\xi)}(\mathbf{p}) &= \int H_k^{(\xi)}(\mathbf{p})d\xi \\ &= \frac{\left(r_k^2 + c^2\right)^{\frac{3}{2}}}{6} + \frac{r_k^2 - \left(\xi_{\mathbf{p}} - \xi_{\mathbf{p}_k}\right)^2 + c^2}{2} \left(\xi_{\mathbf{p}} - \xi_{\mathbf{p}_k}\right) \ln\left(\xi_{\mathbf{p}} - \xi_{\mathbf{p}_k} + \sqrt{r_k^2 + c^2}\right). \\ &\quad - \frac{r_k^2 - \left(\xi_{\mathbf{p}} - \xi_{\mathbf{p}_k}\right)^2 + c^2}{2} \sqrt{r_k^2 + c^2}. \end{aligned} \tag{13}$$

With the omission of the polynomial for the term $\bar{H}_k(\mathbf{p})$, the approximation of u by this method can be written as

$$u(\mathbf{p}) = \sum_{k=1}^{N} \mu_k \bar{H}_k(\mathbf{p}). \tag{14}$$

Equation (14) is discovered to have N freedoms in the current method, which can be used to construct an $N-$ dimensional linear vector space. In this equation, $\left\{\bar{H}_k\left(\mathbf{p}\right), k=1,2,...,N\right\}$ forms a set of base functions in V_N . As a result, the weighting coefficients $w_{ij}^{(n,\xi)}$ can be calculated in the same manner as in Section 2.1 and are represented by the following formula:

$$\vec{w}_i^{(n,\xi)} = \left[B\right]^{-1} \frac{\partial^{(n)} \vec{\bar{H}}\left(\mathbf{p}_i\right)}{\partial \xi^{(n)}}, \quad i=1,2,...,N, \tag{15}$$

Where

$$\left[B\right] = \begin{bmatrix} \bar{H}_1(\mathbf{p}_1) & \bar{H}_1(\mathbf{p}_2) & \cdots & \bar{H}_1(\mathbf{p}_N) \\ \bar{H}_2(\mathbf{p}_1) & \bar{H}_2(\mathbf{p}_2) & \cdots & \bar{H}_2(\mathbf{p}_N) \\ & & \ddots & \\ \bar{H}_N(\mathbf{p}_1) & \bar{H}_N(\mathbf{p}_2) & \cdots & \bar{H}_N(\mathbf{p}_N) \end{bmatrix}. \tag{16}$$

Considering that we differentiate φ 's integrated form, the approach is referred to as the "Indirect method (iDR)."

3. IMPLEMENTATION TO THE TIME-DEPENDENT CONVECTION-DIFFUSION PROBLEMS

In this work, two-dimensional convection-diffusion problems defined on domain Ω with boundary Γ that are modeled and governed by the following partial differential equation are to be numerically solved. Implementation to the time-dependent convection-diffusion problems

$$\frac{\partial u}{\partial t} + V_x \frac{\partial u}{\partial x} + V_y \frac{\partial u}{\partial y} = \varepsilon_x \frac{\partial^2 u}{\partial x^2} + \varepsilon_y \frac{\partial^2 u}{\partial y^2} - \beta u + g\left(x,y,t\right), \tag{17}$$

where ε_x and ε_y are diffusion coefficients and V_x and V_y are convection coefficients. The final two terms β and the source term $g\left(x,y,t\right)$ are optional and only required in certain cases. The following initial condition is given

$$u\left(\mathbf{p},t_0\right) = \psi_1(\mathbf{p}), \mathbf{p} \in \Omega \cup \Gamma. \tag{18}$$

With also the boundary condition expressed as follows

$$u\left(\mathbf{p},t\right) = \psi_2(\mathbf{p},t), t \geq t_0 \ , \mathbf{p} \in \Gamma.. \tag{19}$$

In this work, the main attention is paid to problems in two dimensions only, hence for $\mathbf{p} \in \Omega \cup \Gamma$,

$$\mathbf{p} = \left(x,y\right). \tag{20}$$

The two collocation meshfree methods, DR and iDR, previously detailed in the previous section are now implemented to the above equation. For the transient problem, one of the most often used techniques for finding numerical solutions to time dependent partial differential equations is the forward time stepping strategy and it is used in this work. The time discretization for $t \in \left(t_0, t_0 + \Delta t\right]$ is approximated as follows

$$\begin{aligned}&\frac{\partial u}{\partial t}\approx\frac{u_t-u_{t-\Delta t}}{\Delta t},\quad \frac{\partial u}{\partial x}\approx\frac{\partial u_{t-\Delta t}}{\partial x},\quad \frac{\partial u}{\partial y}\approx\frac{\partial u_{t-\Delta t}}{\partial y},\\&\frac{\partial^2 u}{\partial x^2}\approx\frac{\partial^2 u_{t-\Delta t}}{\partial x^2},\quad \frac{\partial^2 u}{\partial y^2}\approx\frac{\partial^2 u_{t-\Delta t}}{\partial y^2}.\end{aligned}\tag{21}$$

By substituting back into Equation (17), the following statement can be further proceeded,

$$\begin{aligned}u(\mathbf{p},t)=u(x,y,t)\approx u_{t-\Delta t}+\Delta t\Bigg(&\varepsilon_x\frac{\partial^2 u_{t-\Delta t}}{\partial x^2}+\varepsilon_y\frac{\partial^2 u_{t-\Delta t}}{\partial y^2}\\&-V_x\frac{\partial u_{t-\Delta t}}{\partial x}-V_y\frac{\partial u_{t-\Delta t}}{\partial y}-\beta u_{t-\Delta t}+g_{t-\Delta t}(\mathbf{p})\Bigg).\end{aligned}\tag{22}$$

Equation (8) is substituted into Equation (22) to produce

$$\begin{aligned}u(\mathbf{p}_i,t)\approx u_{t-\Delta t}(\mathbf{p}_i)+\Delta t\Bigg(&\varepsilon_x\sum_{j=1}^{N}w_{ij}^{(2,x)}u_{t-\Delta t}(\mathbf{p}_j)+\varepsilon_y\sum_{j=1}^{N}w_{ij}^{(2,y)}u_{t-\Delta t}(\mathbf{p}_j)\\&-V_x\sum_{j=1}^{N}w_{ij}^{(1,x)}u_{t-\Delta t}(\mathbf{p}_j)-V_y\sum_{j=1}^{N}w_{ij}^{(1,y)}u_{t-\Delta t}(\mathbf{p}_j)-\beta u_{t-\Delta t}(\mathbf{p}_i)+g_{t-\Delta t}(\mathbf{p}_i)\Bigg),\end{aligned}\tag{23}$$

for $i=1,2,...,N.$

Therefore, for each $\mathbf{p}_i$, it leads to

$$\begin{aligned}\mathbf{U}_t\approx\mathbf{U}_{t-\Delta t}+\Delta t\Big(&\varepsilon_x\mathbf{w}^{(2,x)}\mathbf{U}_{t-\Delta t}+\varepsilon_y\mathbf{w}^{(2,y)}\mathbf{U}_{t-\Delta t}\\&-V_x\mathbf{w}^{(1,x)}\mathbf{U}_{t-\Delta t}-V_y\mathbf{w}^{(1,y)}\mathbf{U}_{t-\Delta t}-\beta\mathbf{U}_{t-\Delta t}+\mathbf{g}_{t-\Delta t}\Big).\end{aligned}\tag{24}$$

where $\mathbf{U}_t=\left[u(\mathbf{p}_1,t),u(\mathbf{p}_2,t),...,u(\mathbf{p}_N,t)\right]^T$,

$\mathbf{U}_{t-\Delta t}=\left[u(\mathbf{p}_1,t-\Delta t),u(\mathbf{p}_2,t-\Delta t),...,u(\mathbf{p}_N,t-\Delta t)\right]^T$,

$\mathbf{g}_{t-\Delta t}=\left[g(\mathbf{p}_1,t-\Delta t),g(\mathbf{p}_2,t-\Delta t),...,g(\mathbf{p}_N,t-\Delta t)\right]^T$

and $\mathbf{w}^{(n,\xi)}=\left[\vec{w}_1^{(n,\xi)}\mid\vec{w}_2^{(n,\xi)}\mid...\mid\vec{w}_N^{(n,\xi)}\right]^T$ which can be briefly provided for the two different meshless methods as follows.

- For the direct method (DR) it is of the following form

$$\mathbf{w}^{(n,x)}=\begin{bmatrix}\sum_{j=1}^{N}a_{1j}\frac{\partial^{(n)}\varphi_j(\mathbf{p}_1)}{\partial x^{(n)}} & \sum_{j=1}^{N}a_{2j}\frac{\partial^{(n)}\varphi_j(\mathbf{p}_1)}{\partial x^{(n)}} & \cdots & \sum_{j=1}^{N}a_{Nj}\frac{\partial^{(n)}\varphi_j(\mathbf{p}_1)}{\partial x^{(n)}}\\ \sum_{j=1}^{N}a_{1j}\frac{\partial^{(n)}\varphi_j(\mathbf{p}_2)}{\partial x^{(n)}} & \sum_{j=1}^{N}a_{2j}\frac{\partial^{(n)}\varphi_j(\mathbf{p}_2)}{\partial x^{(n)}} & \cdots & \sum_{j=1}^{N}a_{Nj}\frac{\partial^{(n)}\varphi_j(\mathbf{p}_2)}{\partial x^{(n)}}\\ & & \ddots & \\ \sum_{j=1}^{N}a_{1j}\frac{\partial^{(n)}\varphi_j(\mathbf{p}_N)}{\partial x^{(n)}} & \sum_{j=1}^{N}a_{2j}\frac{\partial^{(n)}\varphi_j(\mathbf{p}_N)}{\partial x^{(n)}} & \cdots & \sum_{j=1}^{N}a_{Nj}\frac{\partial^{(n)}\varphi_j(\mathbf{p}_N)}{\partial x^{(n)}}\end{bmatrix},$$

where a_{1j} are elements of $\left[A\right]^{-1}$ in Equation (7).

- For the indirect method (iDR) it is of the following form

$$\mathbf{w}^{(n,x)}=\begin{bmatrix}\sum_{j=1}^{N}b_{1j}\dfrac{\partial^{(n)}\bar{H}_j(\mathbf{p}_1)}{\partial x^{(n)}} & \sum_{j=1}^{N}b_{2j}\dfrac{\partial^{(n)}\bar{H}_j(\mathbf{p}_1)}{\partial x^{(n)}} & \cdots & \sum_{j=1}^{N}b_{Nj}\dfrac{\partial^{(n)}\bar{H}_j(\mathbf{p}_1)}{\partial x^{(n)}}\\ \sum_{j=1}^{N}b_{1j}\dfrac{\partial^{(n)}\bar{H}_j(\mathbf{p}_2)}{\partial x^{(n)}} & \sum_{j=1}^{N}b_{2j}\dfrac{\partial^{(n)}\bar{H}_j(\mathbf{p}_2)}{\partial x^{(n)}} & \cdots & \sum_{j=1}^{N}b_{Nj}\dfrac{\partial^{(n)}\bar{H}_j(\mathbf{p}_2)}{\partial x^{(n)}}\\ & & \ddots & \\ \sum_{j=1}^{N}b_{1j}\dfrac{\partial^{(n)}\bar{H}_j(\mathbf{p}_N)}{\partial x^{(n)}} & \sum_{j=1}^{N}b_{2j}\dfrac{\partial^{(n)}\bar{H}_j(\mathbf{p}_N)}{\partial x^{(n)}} & \cdots & \sum_{j=1}^{N}b_{Nj}\dfrac{\partial^{(n)}\bar{H}_j(\mathbf{p}_N)}{\partial x^{(n)}}\end{bmatrix},$$

where b_{1j} are elements of $\left[B\right]^{-1}$ in Equation (15).

4. NUMERICAL COMPONENTS

4.1. The algorithm

Step 1. Generate the set of points $\{\mathbf{p}\}_{i=1}^{N}$ in the domain $\Omega\cup\Gamma$ and divide it into two non-intersecting sets: the set of interior points on Ω ($\{\mathbf{p}\}_{i=1}^{Ni}$, containing N_i elements), and the set of boundary points on Γ ($\{\mathbf{p}\}_{i=N_i+1}^{N_i+Nb}$, containing N_b elements), where $N_i+N_b=N.$

Step 2. Calculate the matrices $\mathbf{w}^{(1,x)}$, $\mathbf{w}^{(2,x)}$, $\mathbf{w}^{(1,x)}$ and $\mathbf{w}^{(2,y)}$ using the format should be calculated with $\mathbf{w}^{(n,\xi)}=\left[\vec{w}_1^{(n,\xi)}\,|\,\vec{w}_2^{(n,\xi)}\,|\ldots|\,\vec{w}_N^{(n,\xi)}\right]^T$.

- The vector $\vec{w}_i^{(n,\xi)}$ is taken on the form of Equation (7), for $i=1,2,...,N,$ for DR method.
- It is of the form of Equation (15) for $i=1,2,...,N,$ if the iDR is under consideration.

Step 3. The following operations are carried out during each iteration.

3.1. Apply the initial condition at $t=t_0$ by specifying the following.

$$u(\mathbf{p}_i)=\psi_1(\mathbf{p}_i),\ \text{for}\ i=1,2,...,N.$$

3.2. Apply the boundary conditions.

$$u(\mathbf{p}_i)=\psi_2(\mathbf{p}_i,t),\ \text{for}\ i=N_i+1,N_i+2,...,N_i+N_b\ \text{and}\ t\geq t_0.$$

3.3. Use Equation (23) to determine the approximate value of $u(\mathbf{p}_i,t)$, for $i=1,2,...,N.$

3.4. For the next time step, setting

$$u(\mathbf{p}_i,t-\Delta t)\leftarrow u(\mathbf{p}_i,t)\ \text{for}\ i=1,2,...,N,\ \text{and}\ t-\Delta t\leftarrow t.$$

Step 4. The calculation comes to an end at $t=t_{end}$.

Therefore, the approximate values of $u(\mathbf{p}_i, t_{end})$ is now obtained.

Step 5. Validate the approximate solution using the following criteria.

4.2. Solution validation criteria

Regarding the quality of the solutions obtained from the two proposed meshless methods, the first criterion is on the accuracy and two error measurements (defined for a location $\mathbf{p}_i$ at time t) are employed.

1. The relative error norm ($Rel.Err$), defined as

$$Rel.Err = \sqrt{\frac{\sum_{i=1}^{N}(u^{exact}(\mathbf{p}_i,t)-u^{num}(\mathbf{p}_i,t))^2}{\sum_{i=1}^{N}\left(u^{exact}(\mathbf{p}_i,t)\right)^2}}, \tag{25}$$

2. The root mean square error (RMSE), defined as

$$\text{RMSE} = \sqrt{\frac{1}{N}\sum_{i=1}^{N}\left(u^{exact}(\mathbf{p}_i,t)-u^{num}(\mathbf{p}_i,t)\right)^2}, \tag{26}$$

where $u^{exact}(\mathbf{p}_i,t)$ is the exact solution and $u^{num}(\mathbf{p}_i,t)$ is the numerical one, both measured at node $\mathbf{p}_i$ and a target/final time t. The results obtained through this work are verified against their exact ones and those found in literature, if available. Additionally, it is of interest to observe the issue related to the use of RBF-based numerical techniques which is the sensitivity to shape parameter.

5. NUMERICAL EXPERIMENTS WITH RESULTS AND GENERAL DISCUSSION

5.1. Example 1

To test out the two meshless methods, let's firstly examine a dimensionless diffusion equation in this example, as provided in [66],

$$\frac{\partial u}{\partial t} = \frac{\partial^2 u}{\partial x^2} + \frac{\partial^2 u}{\partial y^2}. \tag{27}$$

The assumption is that the problem domain is a square domain $\mathbf{p} \in [-0.5, 0.5] \times [-0.5, 0.5]$, the initial condition is $u(\mathbf{p}, t_0) = 1$ and Dirichlet jump boundary condition is $u(\mathbf{p}, t) = 0.$ The exact solution is given by [67], expressed as follows

$$u(\mathbf{p},t) = \frac{16}{\pi^2} u_{exact}(x,t) u_{exact}(y,t), \tag{28}$$

with $\xi = x$ or y. The following is obtained,

$$u_{exact}(\xi,t) = \sum_{i=0}^{\infty} \frac{(-1)^i \exp\left[-(2i+1)^2 \pi^2 t\right] \cos\left[(2i+1)\pi\xi\right]}{2i+1}. \tag{29}$$

In examining radial basis function (RBF)-based approaches, the impact of the 'shape parameter, (c)' emerges as a fundamental aspect. This is substantiated in Figure 1, which presents a detailed analysis of the root mean square

error (RMSE) across different shape parameter values in two non-grid-based (meshless) methods at two distinct time intervals, $t = 10^{-2}$ and $t = 10^{-3}$. A key observation from this analysis is the identification of an optimal range for the shape parameter, roughly between 0.25 and 0.75. Within this interval, the RMSE maintains lower levels, indicating more accurate results. Conversely, shape parameter values outside this range result in significantly higher error levels. An additional noteworthy trend is the inverse relationship between the magnitude of the shape parameter and the accuracy of both evaluated schemes, DR and iDR. This highlights the critical influence of the shape parameter on the performance and reliability of RBF-based computational methods.

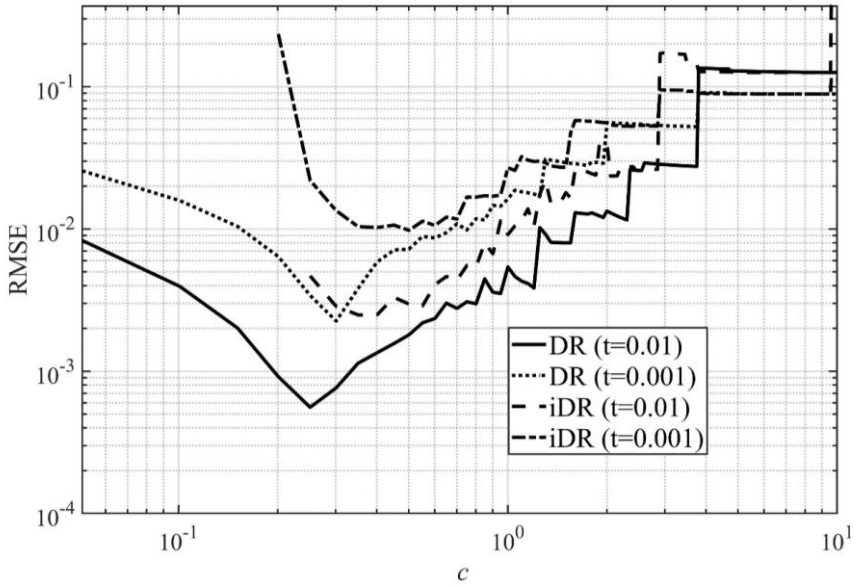

Figure 1: Root mean square error (RMSE) measured at different shape values (c) produced by the two meshless methods at two target times: $t = 0.01$ and 0.001.

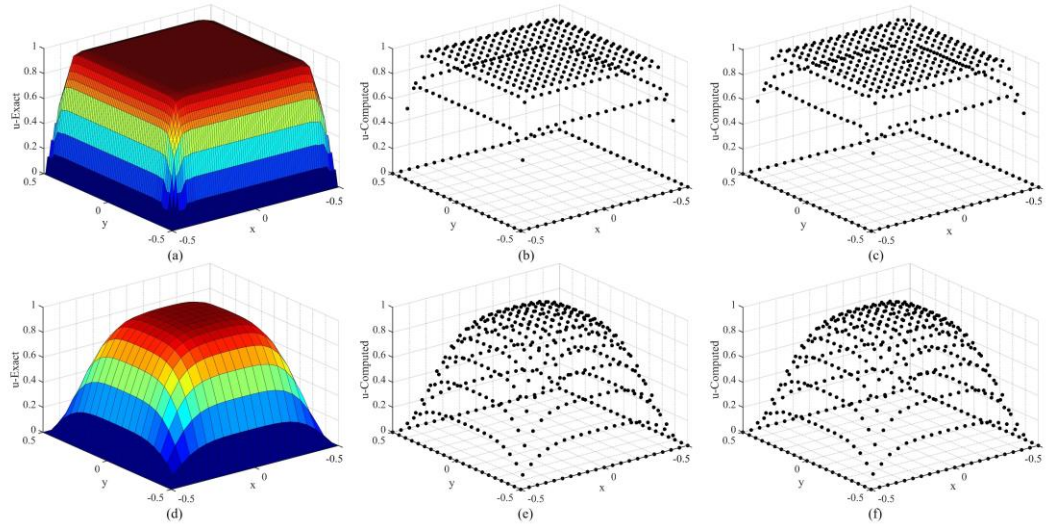

Figure 2: Solution profiles using $\Delta t = 0.0001$ and $N = 21 \times 21$: First row at $t = 0.01$; (a) the exact, (b) DR with $c = 0.301$, and (c) iDR with $c = 0.501$. Second row at $t = 0.001$; (d) the exact, (e) DR with $c = 0.251$, and (f) iDR with $c = 0.351$.

In the conducted study, as depicted in Figure 2, the comparative analysis of solution profiles generated by two distinct meshless methodologies is presented. These profiles were evaluated at two temporal junctures,

specifically at $t=10^{-2}$ and $t=10^{-3}$. Each graphical representation in the figure adheres to the most effective shape parameter, maintaining a constant time step size of $\Delta t=10^{-4}$ and a uniform node density configured at $N=21\times 21$. Initial observations indicate a pronounced gradient in the flow variable along the peripheries at the onset of the phenomenon, which progressively smoothens as time advances.

Quantitatively, at the $t=10^{-2}$ interval, the DR meshless approach registers RMSE values of $RMSE=2.26E-03$ and $Rel.Err=2.63E-03$. In contrast, the iDR methodology yields RMSE figures of $RMSE=9.79E-03$ and $Rel.Err=1.14E-02$. Advancing the temporal frame to $t=10^{-3}$, the DR method demonstrates RMSE values of $RMSE=5.58E-04$ and $Rel.Err=8.61E-04$, while the iDR approach results in RMSE values of $RMSE=2.49E-03$ and $Rel.Err=3.84E-03$. This initial numerical experimentation allows for the inference that, given the utilization of an optimal shape parameter, the DR methodology exhibits marginally superior accuracy in comparison to the iDR approach.

Upon comparison with the results documented in [66], it is observed that the overall performance, in terms of accuracy, is approximately equivalent. It is important to note, however, that the comparable quality of approximate solutions achieved in their study was facilitated by the use of a significantly denser node grid, namely a 51×51 configuration. This distinction may be attributed to the localized nature of the collocation methods employed in their research, which markedly contrasts with the global methodology developed and implemented in our present study.

5.2. Example 2

In this example, the problem investigated in [54, 68] is numerically solved. In this case, the convection and diffusion coefficients are both set to constant values of $V_x=V_y=0.8$ and $\varepsilon_x=\varepsilon_y=0.01$, respectively, with $g(x)=\beta=0$. The exact solution is provided as follows

$$u(\mathbf{p},t)=\frac{1}{4t+1}\exp\left(-\left[\frac{(x-0.8t-0.5)^2}{0.01(4t+1)}+\frac{(y-0.8t-0.5)^2}{0.01(4t+1)}\right]\right). \tag{30}$$

The exact is defined over a square domain $\mathbf{p}\in[0.5,2]\times[0.5,2]$ and is used as the source for both the initial and boundary conditions.

In Table 1, an evaluation is presented on the performance of two meshfree methods, with a focus on relative errors ($Rel.Err$) over time progression. This assessment encompasses a range of time step sizes, specifically Δt values of 10^{-2}, 10^{-3} and 10^{-4}. The results demonstrate a high degree of alignment between the approximate solutions provided by these methods and the exact solutions, consistent across all target times and the mentioned Δt increments. Nevertheless, there are distinct patterns in the trends of their solutions. A key observation is the improvement in accuracy as the time step sizes decrease, particularly evident for most of the selected target times. However, a notable exception is observed in the longitudinal performance of the simulations. Generally, a gradual decline in accuracy is noted as time progresses. This trend is interrupted in two specific cases involving the DR method with Δt values of 10^{-3} and 10^{-4}. In these instances, there is a surprising reduction in relative errors, highlighting an area of interest for further study into the behavior of the DR method under such parameters.

In the comparative analysis of the efficacy of two meshless methodologies, an examination of Figure 3 elucidates the accuracy trends correlated with incremental node density enhancement, spanning from $N=10\times 10, 15\times 15$ to 20×20, at successive time steps within the range of 0.10 – 1.00. The data distinctly demonstrates that across

all node dimensions, the DR method exhibits superior performance over the iDR approach. Notably, DR maintains consistent accuracy irrespective of node size variations and temporal progression, though minor fluctuations are observable with coarser nodes at initial timeframes. Further corroboration of DR's predominance over iDR is evident in its sustained accuracy in tracking the moving pulse over time, as illustrated in Figure 4. This figure reveals that while both methods yield reasonable phase alignment of the pulse, the amplitude replication is notably deficient in the iDR method, as delineated in Figure 4(i).

In accordance with the findings delineated in [54], it is intriguingly observed that the utilization of globally derived numerical approaches yields a performance superior to that achieved in the current study. This disparity in outcomes may be ascribed to the selection of Radial Basis Functions (RBFs) used, particularly the inverse variant of Multiquadric (MQ), as implemented in their investigation. This aspect presents a potential avenue for further investigation in our subsequent research endeavors. Additionally, both studies exhibit a similar trend of error increment over time, which is consistent in most instances. In contrast to [68], it is important to acknowledge that although the nature of the problem being investigated remains consistent, the specific details of the problem, particularly the range of the convection and diffusion coefficients, are significantly distinct. Furthermore, the numerical scheme employed in their research was developed at a considerably higher order and executed without incorporating Radial Basis Functions. Despite these differences, both studies benchmark their performance against the exact solution form, which is a reasonable approach. It should be duly noted that this concise yet noteworthy observation is also applicable to the subsequent example.

Table 1: Relative errors ($Rel.Err$) progression at each time $t \in (0,1]$, computed using $N = 15 \times 15$ and three time step sizes $\Delta t = 10^{-2}, 10^{-3}$, and 10^{-4}

t	$\Delta t = 0.01$		$\Delta t = 0.001$		$\Delta t = 0.0001$	
	DR ($c = 0.36$)	iDR ($c = 2.39$)	DR ($c = 0.36$)	iDR ($c = 2.39$)	DR ($c = 0.36$)	iDR ($c = 2.39$)
0.1	1.507E-01	3.021E-01	1.482E-01	3.093E-01	1.483E-01	3.101E-01
0.2	1.261E-01	3.110E-01	1.074E-01	3.189E-01	1.081E-01	3.200E-01
0.3	1.731E-01	4.296E-01	1.253E-01	4.076E-01	1.252E-01	4.060E-01
0.4	1.893E-01	4.931E-01	1.049E-01	4.566E-01	1.046E-01	4.539E-01
0.5	2.132E-01	5.377E-01	9.191E-02	4.949E-01	9.082E-02	4.919E-01
0.6	2.355E-01	6.215E-01	8.103E-02	5.577E-01	7.914E-02	5.530E-01
0.7	2.562E-01	7.234E-01	7.278E-02	6.300E-01	6.998E-02	6.230E-01
0.8	2.748E-01	7.674E-01	6.653E-02	6.573E-01	6.277E-02	6.494E-01
0.9	2.913E-01	7.453E-01	6.167E-02	6.303E-01	5.694E-02	6.228E-01
1.0	3.059E-01	7.408E-01	5.782E-02	6.218E-01	5.212E-02	6.149E-01

International Journal of Multiphysics
Volume 18, No. 2s, 2024
ISSN: 1750-9548

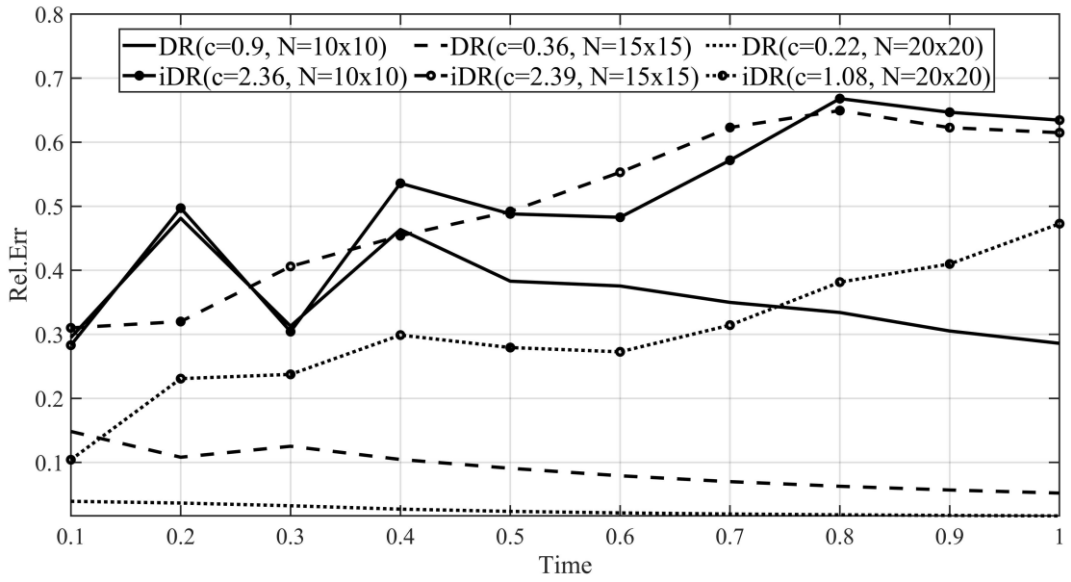

Figure 3: Relative error ($Rel.Err$) measured at different target times for the two meshless methods at three levels of node density; $N = 10\times10,\ 15\times15,$ and 20×20.

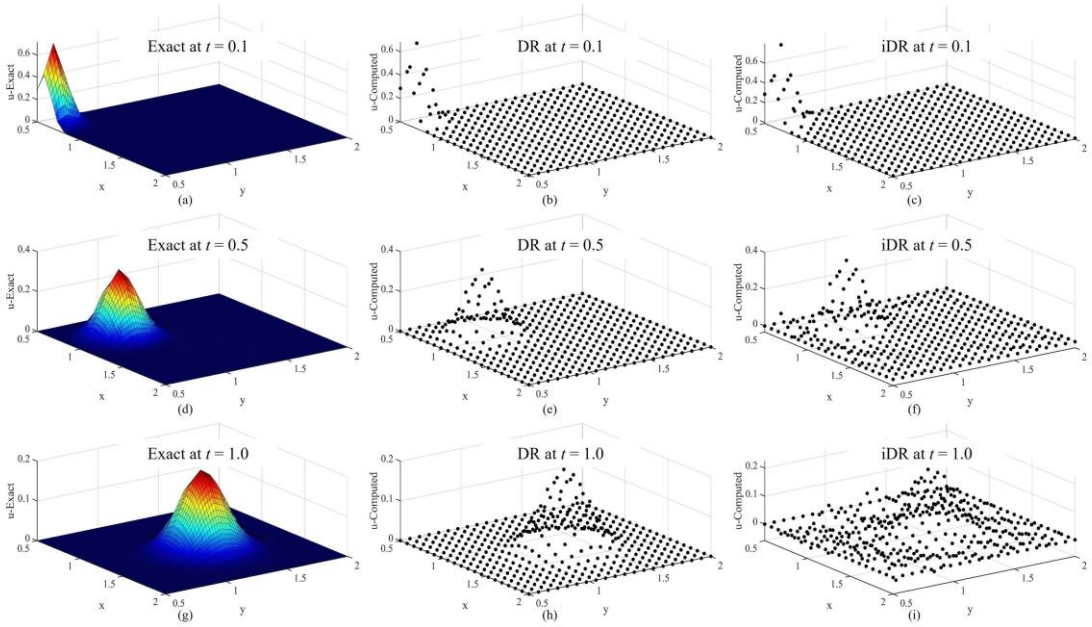

Figure 4: Approximation of the moving pulse with the two meshless methods at $t = \{0.1, 0.5, 1.0\}$, using $\Delta t = 0.0001$ and $N = 20\times20$; (a-d-g) Exact, (b-e-h) DR with $c = 0.22$, and (c-f-i) iDR with $c = 0.18$.

5.3. Example 3

Another challenging problem is that investigated in [54, 68] where the governing equation is the same as previously investigated in Example 2, except that $\beta = 0$ with the following the source term

$$g(\mathbf{p},t)=\cos\left(\varepsilon_x x+\varepsilon_y y\right)\left(\varepsilon_x V_x+\varepsilon_y V_y\right)\exp(-t\left(\left(\varepsilon_x\right)^3+\left(\varepsilon_y\right)^3\right)). \quad (31)$$

All boundary conditions are taken from the analytical solution, which is given as follows,

$$u(\mathbf{p},t)=\sin\left(\varepsilon_x x+\varepsilon_y y\right)\exp(-t\left(\left(\varepsilon_x\right)^3+\left(\varepsilon_y\right)^3\right)). \quad (32)$$

The problem is defined on the computational domain $\Omega\cup\Gamma=[0,2]\times[0,2]$.

In the present study, the investigation focuses on analyzing the capability of different approaches to address convection-dominated scenarios. This is achieved by incorporating the Péclet number (Pe), a crucial metric representing the convection to diffusion rate ratio. The escalation of Pe poses a significant challenge for numerical methodologies, a phenomenon explored in this research through the amplification of convection coefficients, V , in both directions. Maintaining a constant diffusion coefficient, the study presents in Table 2 the approximate solutions derived from two distinct schemes. These solutions are calculated at $t=0.01$, utilizing a $\Delta t=0.0001$ and examining three varying node densities ($N=7\times7, 13\times13,$ and 23×23), across a V range of 100 to 400. The results elucidate a gradual decline in accuracy for both methods as the scenarios become increasingly convection-dominated, a pattern consistent across all node sizes examined. Interestingly, at lower node densities, the indirect method (iDR) demonstrates a marginally superior performance compared to the direct method (DR) as V escalates. Conversely, this trend reverses with the inclusion of a greater number of nodes.

In advanced thermal dynamics research, where convection coefficients surpass certain thresholds (specifically), the focus shifts to examining higher coefficients, such as $V=500$. This investigation is captured in Figure 5, which presents numerical solutions along the $x=y$ axis, recorded at a specific time frame of $t=0.01$. This analysis utilizes a time step of $\Delta t=0.0001$, incorporating three different levels of node density for comprehensive evaluation. The study compares two methodologies: Direct Representation (DR) and indirect Direct Representation (iDR). The results demonstrate a significant alignment of both methods with the exact solutions, maintaining this consistency across varying node sizes. In contrast, analysis along the line $x=2-y$, detailed in Figure 6, reveals a distinctive insight. Here, the direct method proves more effective than its indirect counterpart in addressing instabilities at boundary layers, especially at corner points, under conditions of high Péclet numbers (Pe =600). This phenomenon continues to be evident in scenarios extending beyond these specific conditions, though such results are not included in this report.

In the context of simulation duration, Table 3 presents the computational time (Ctm.) in seconds across various $V_x=V_y=V$, $\varepsilon_x=\varepsilon_y=1$ settings, alongside node refinement at $t=0.01$ and $\Delta t=0.0001$. This data reveals that iDR consistently demands around 50% less time compared to DR, irrespective of the Pe values and the scale of computational nodes. Additionally, it should be noted that the values showcased in this instance derive from a somewhat improvised selection of the optimal shape parameter.

Table 2: Relative error ($Rel.Err$) revealed from each RBF at different values $V_x=V_y=V$, $\varepsilon_x=\varepsilon_y=1$, and nodes refinement (N) at $t=0.01$ and $\Delta t=0.0001$

$Rel.Err$	$N=7\times7$		$N=13\times13$		$N=23\times23$	
	DR ($c=3$)	iDR ($c=4.6$)	DR ($c=3$)	iDR ($c=4.6$)	DR ($c=3$)	iDR ($c=3.5$)
V=100	2.922E-04	8.081E-05	1.889E-05	6.966E-05	1.620E-05	1.624E-04
V=200	8.209E-04	2.637E-04	3.165E-05	1.373E-04	3.169E-05	3.892E-04
V=300	1.120E-03	3.583E-04	1.420E-04	2.030E-04	5.908E-05	6.687E-04
V=400	3.713E-03	1.551E-03	3.034E-03	4.161E-04	8.926E-04	1.151E-03

Table 3: Computational time (Ctm.) (in seconds) revealed from each meshless method at different values $V_x = V_y = V$, $\varepsilon_x = \varepsilon_y = 1$ and nodes refinement (N) at $t = 0.01$ and $\Delta t = 0.0001$

Ctm.	$N = 7\times 7$		$N = 13\times 13$		$N = 23\times 23$	
	DR ($c = 3$)	iDR ($c = 4.6$)	DR ($c = 3$)	iDR ($c = 4.6$)	DR ($c = 3$)	iDR ($c = 3.5$)
V=100	8.084E-02	4.547E-01	9.374E-01	4.307E-01	8.872E+00	3.011E+00
V=200	8.221E-02	1.387E-01	9.039E-01	4.148E-01	8.814E+00	2.430E+00
V=300	8.179E-02	1.518E-01	8.935E-01	4.322E-01	8.683E+00	2.115E+00
V=400	8.291E-02	1.512E-01	8.959E-01	4.413E-01	8.911E+00	3.196E+00

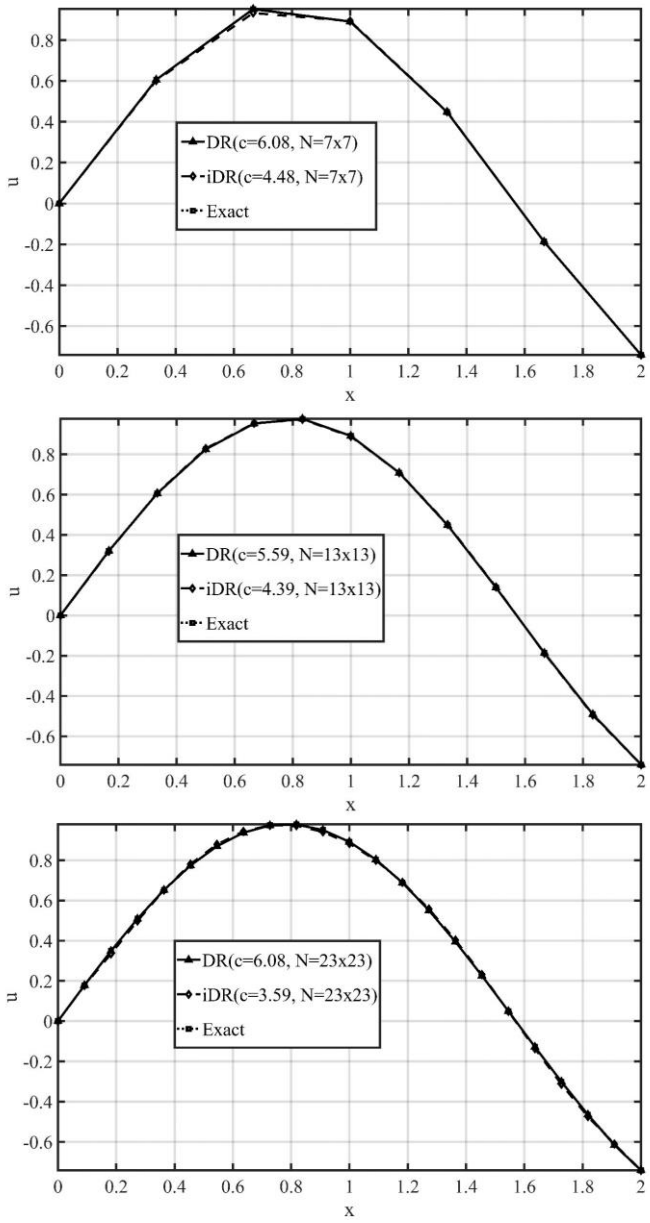

Figure 5: Solution comparison computed on the $x = y$ straight line for $V_x, = V_y, = 500, \quad \varepsilon_x = \varepsilon_y = 1$ recorded at $t = 0.01$ using $\Delta t = 0.0001$ with three levels of node densities.

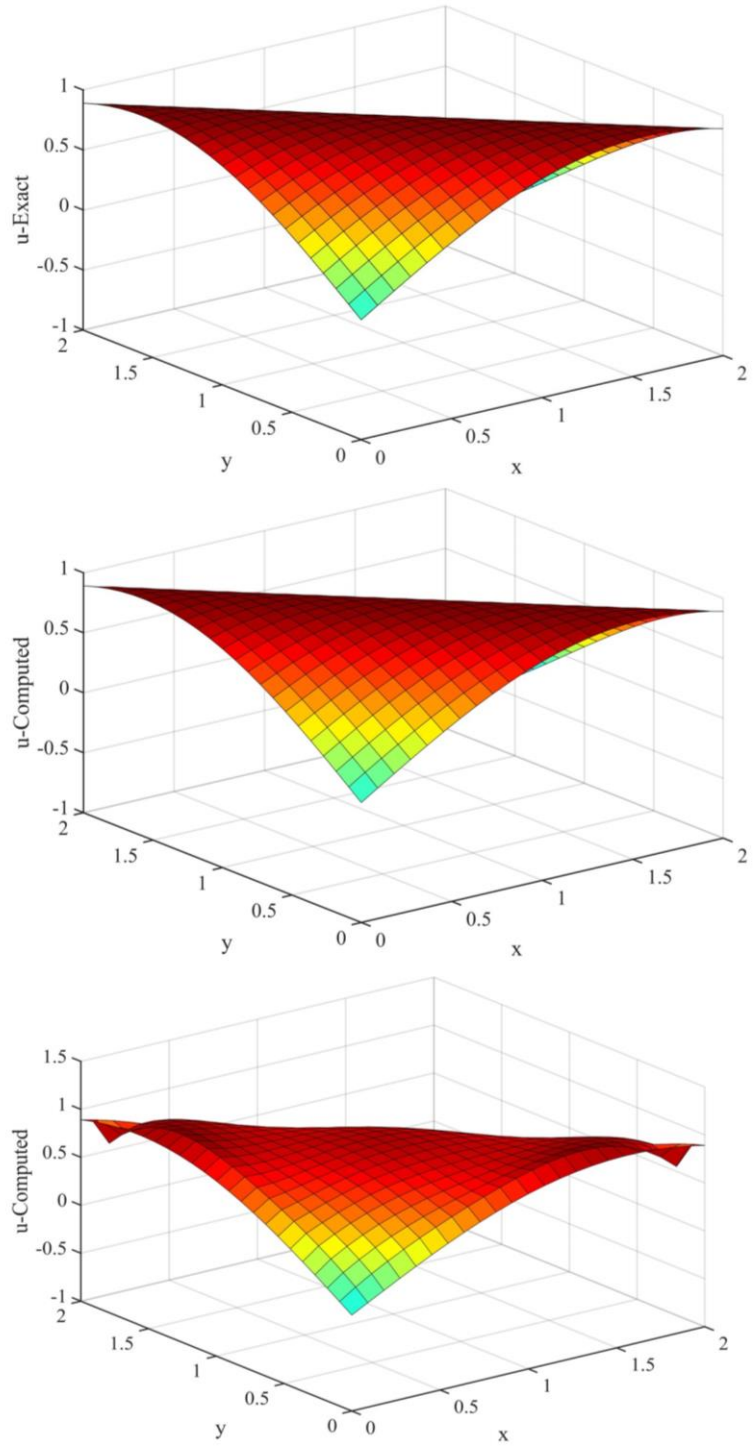

Figure 6: Solution surface plots computed for $V_x, = V_y, = 600,\ \varepsilon_x = \varepsilon_y = 1$ at $t = 0.01$ and $\Delta t = 0.0001$ with $N = 23 \times 23$; (top) exact, (middle) DR, and (bottom) iDR.

5.4. Example 4

As the last experiment, the problem that [29, 54, 69] mentioned and numerically examined which is the linear advection-diffusion equation, expressed below, is tackled,

$$\frac{\partial u}{\partial t}=\varepsilon_x\frac{\partial^2 u}{\partial x^2}+\varepsilon_y\frac{\partial^2 u}{\partial y^2}+V_x\frac{\partial u}{\partial x}+V_y\frac{\partial u}{\partial y}, \tag{33}$$

where each of $V_x, V_y = V$, $\varepsilon_x = \varepsilon_y = \varepsilon$ is a constant. The problem domain is assumed to be a square domain $\mathbf{p}\in[0,1]\times[0,1]$, and the initial condition is $u(\mathbf{p},t_0)=e^{-C_x x}+e^{-C_y y}$, and the Dirichlet boundary conditions are defined as follows

$$u(\mathbf{p},t)=e^t\left(e^{-C_x x}+e^{-C_y y}\right), \tag{34}$$

where $C_x=\left(V_x+\sqrt{(V_x)^2+4\varepsilon_x}\right)/2\varepsilon_x$ and $C_y=\left(V_y+\sqrt{(V_y)^2+4\varepsilon_y}\right)/2\varepsilon_y$.

In the conducted research, quantitative assessments were performed at specific points utilizing a time step $\Delta t=0.001$, with $V_x=V_y=1$, $\varepsilon_x=\varepsilon_y=0.8$. The time was fixed at $t=0.05$, and a node grid of $N=11\times11$. These results are detailed in Table 4. Upon analysis and comparison with both exact solutions and those found in existing literature ([29] and [54] with different optimal value of shape parameter), it is evident that the implemented methods demonstrate competent performance, yielding results of comparable quality across the selected locations. A recurring challenge in these simulations is the determination of an optimal shape parameter, a dilemma consistent with previous studies. As depicted in Figure 7, the impact of varying node counts ($N=10^2, 15^2, 23^2$) on solution accuracy was explored, particularly concerning shape parameter values ranging from 0.001 to 10.00, applied to both DR and iDR meshless methods. A notable trend observed is the decreasing accuracy of simulations with higher shape parameter values. The optimal range for this parameter appears to be around 1.00. Furthermore, the study reveals that at identical shape parameter values, the DR method slightly outperforms the iDR method in terms of numerical solution accuracy, and a denser node configuration tends to increase error values.

Table 4: Numerical solutions produced by each method (this work and together with some from literature) compared to the exacts; using $\Delta t=0.001$ for $V_x=V_y=1$, $\varepsilon_x=\varepsilon_y=0.8$ and $t=0.05$, using $N=11\times11$.

Internal Node	This work		From literature			Exact
	DR ($c=1.39$)	iDR ($c=1.12$)	DRBEM [54]	IMQ ($c=0.104$)[29]	TPS [29]	
(0.1,0.1)	1.737710	1.737707	-	1.732981	1.737215	1.737696
(0.5,0.1)	1.274223	1.274221	1.26601	1.265541	1.273859	1.274227
(0.9,0.1)	1.057990	1.057992	1.04109	1.053769	1.058015	1.057985
(0.3,0.3)	1.186931	1.186929	-	1.169126	1.186137	1.186949
(0.7,0.3)	0.870357	0.870361	0.89901	0.859154	0.870916	0.870372
(0.1,0.5)	1.274223	1.274239	1.27012	1.265541	1.273859	1.274227
(0.5,0.5)	0.810735	0.810733	-	0.799093	0.811537	0.810757

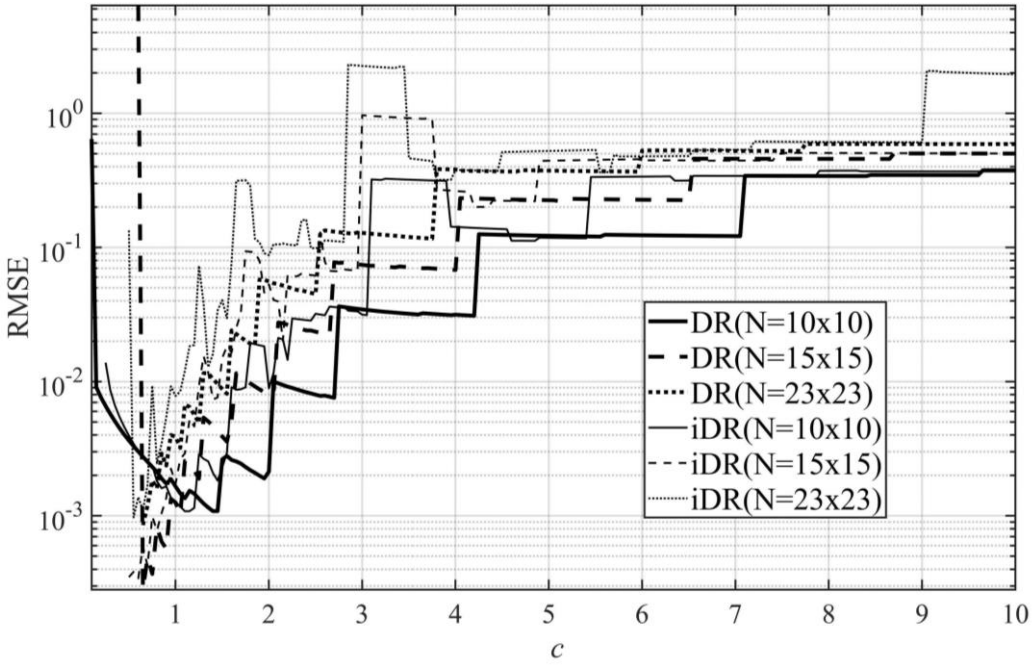

Figure 7: Root mean square error (RMSE) measured at different shape values for the two meshless methods at three levels of node densities: $10\times10, 15\times15$, and 23×23.

In light of the preceding hypothesis regarding the optimal MQ shape parameter, a value of $c = 1.00$ was selected for the study focusing on the enhancement of convection effects. This inquiry involved a series of numerical simulations, utilizing parameters such as $N = 11\times11$, Δt =0.001 and 0.0001, and t =1.00 and 1.50. Additionally, the convection coefficients were incremented across four levels ($V_x = V_y \in \{2, 4, 6, 8\}$), with the outcomes presented in Table 5. A notable observation was the formation of boundary layers along the peripheries concurrent with rising Pe values, which invariably led to a decrease in the accuracy of all approximate solutions under the various simulation conditions employed. Despite this, the overall fidelity of the results was deemed satisfactory, particularly noteworthy were those produced by the DR method (exhibiting a Relative Error less than 0.0001) at $V_x = V_y = 2$ and $t = 1.00$. Comparative analysis of the two time-step sizes featured in this table revealed negligible disparities in result quality within each method. It was observed that the DR method exhibited a consistent, albeit modest, superiority over the iDR method in most scenarios documented.

In a scenario with elevated Pe values, the graphical data presented in Figure 8 provides a comparative analysis of the solution profiles derived from the implementation of two novel meshless methodologies, set side by side against the established exact solutions. The depicted surface visualizations correspond to various temporal markers, specifically $t \in \{0.1, 0.5, 1.0, 1.5\}$, utilizing a time step $\Delta t = 0.0001$ and a nodal distribution of $N = 23\times23$. Observations indicate that both methodologies exhibit a high degree of accuracy in emulating the surface topologies across all examined instances. This trend of precision is consistently maintained, as evidenced by the subsequent analyses for an additional temporal point, $t = 2.0$, as delineated in Figure 9. It is imperative to acknowledge that each simulation was conducted utilizing an ad-hoc 'optimal shape parameter', identified through empirical methodologies.

Table 5: Error measurements recorded at two target times ($t = 1.00, 1.50$) using two time step sizes ($\Delta t = 1.00E-03, 1.00E-04$) for different levels of convection effect ($V_x = V_y \in \{2, 4, 6, 8\}$), simulations produced by a fixed node size of 15×15 using the same shape value $c = 1.00$

$V_x = V_y$ $(\varepsilon_x = \varepsilon_y = 1.4)$	Error norms	Δt	$t = 1.00$		$t = 1.50$	
			DR	iDR	DR	iDR
2	*Rel.Err*	0.001	8.77E-05	1.33E-04	1.07E-04	1.60E-04
		0.0001	8.72E-05	1.32E-04	1.07E-04	1.59E-04
	RMSE	0.001	2.40E-04	3.63E-04	4.82E-04	7.20E-04
		0.0001	2.38E-04	3.60E-04	4.80E-04	7.16E-04
4	*Rel.Err*	0.001	5.20E-04	5.62E-04	6.37E-04	5.92E-04
		0.0001	5.20E-04	5.61E-04	6.38E-04	5.91E-04
	RMSE	0.001	1.08E-03	1.17E-03	2.18E-03	2.03E-03
		0.0001	1.08E-03	1.16E-03	2.18E-03	2.02E-03
6	*Rel.Err*	0.001	2.04E-03	2.36E-03	2.50E-03	2.76E-03
		0.0001	2.04E-03	2.36E-03	2.50E-03	2.76E-03
	RMSE	0.001	3.51E-03	4.07E-03	7.10E-03	7.85E-03
		0.0001	3.51E-03	4.07E-03	7.11E-03	7.85E-03
8	*Rel.Err*	0.001	5.99E-03	7.14E-03	7.35E-03	9.92E-03
		0.0001	6.00E-03	7.15E-03	7.35E-03	9.94E-03
	RMSE	0.001	9.10E-03	1.08E-02	1.84E-02	2.48E-02
		0.0001	9.10E-03	1.08E-02	1.84E-02	2.49E-02

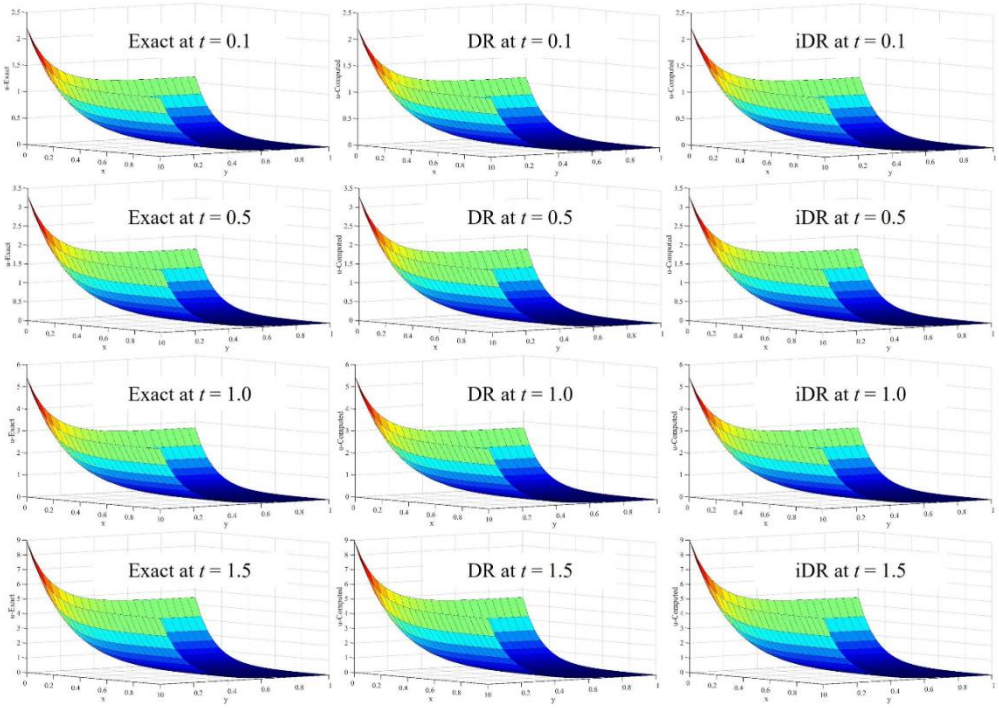

Figure 8: Solution surface plots computed for $V_x, = V_y, = 10, \varepsilon_x = \varepsilon_y = 1.4$ at $t = 0.1$, $t = 0.5$, $t = 1$, $t = 1.5$ using $\Delta t = 0.0001$ and $N = 23 \times 23$ (DR with $c = 0.35$ and iDR with $c = 0.26$).

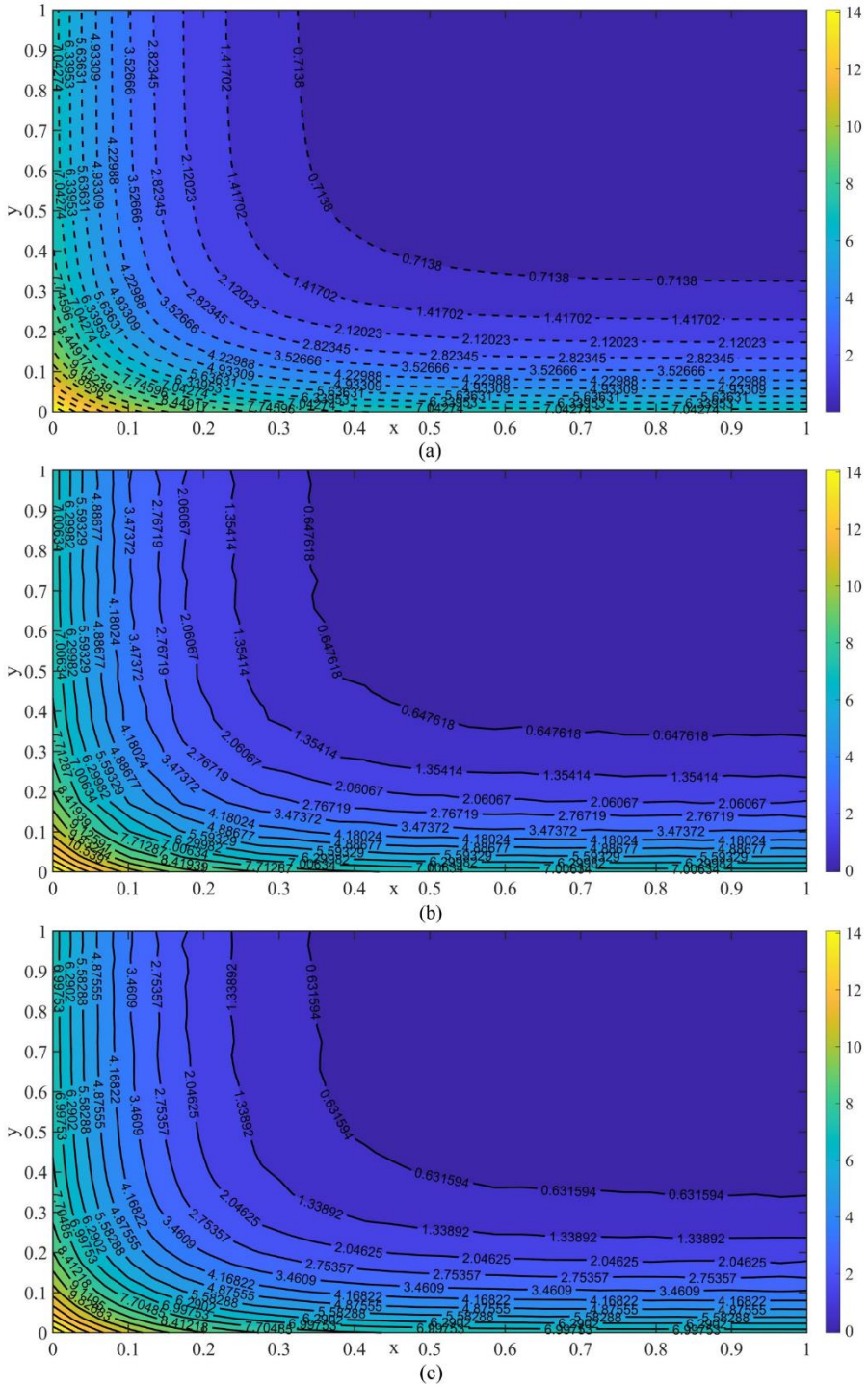

Figure 9: Solution contours obtained for $V_x, = V_y, = 10, \varepsilon_x = \varepsilon_y = 1.4$ measured at $t = 2.0$ using $\Delta t = 0.0001$ and $N = 30 \times 30$; (a) exact, (b) DR with $c = 0.35$, and (c) iDR with $c = 0.26$.

Acknowledgments

The corresponding author would like to express his sincere gratitude to Suranaree University of Technology, Thailand, (Grant no. IRD1-103-64-12-13), for their kind financial support.

6. CONCLUSIONS

This study explores the numerical modelling of the time-dependent convection-diffusion phenomenon in two dimensions, a subject with broad applications in science, engineering, and various other fields. Our primary aim is to apply and compare two mesh-independent numerical schemes: a derivative-based method known as Direct (DR) and an integration-based approach, termed Indirect (iDR). Both these methods are developed utilizing the concept of global collocation, employing the widely recognized multiquadric (MQ) radial basis function (RBF). We explore four test cases in this context, focusing on shape parameter sensitivity, time and node density performance, convection-dominated scenario handling, computational efficiency, and varying node counts and convection effects. The comprehensive analysis encompassing four numerical experiments with meshless methodologies, particularly the Direct (DR) and Indirect (iDR) methods, reveals key insights into their performance under varied conditions. Across the experiments, it is evident that the choice of shape parameter, predominantly within the 0.25 to 0.75 range, significantly influences accuracy, with optimal performance typically observed at around c =1.00. In terms of root mean square error (RMSE), the DR method generally exhibits superior precision, with values ranging from 0.00226 to 0.00558, compared to iDR's 0.00114 to 0.00979, especially in scenarios with smaller time steps (Δt) and higher node densities. The experiments also highlight a consistent trend where accuracy improves with smaller Δt sizes but declines over longer simulation durations. Notably, in convection-dominated scenarios (high Péclet numbers), the DR method tends to outperform iDR, particularly at higher node counts, although iDR shows marginally better performance at lower node densities and demands about 50% less computational time. Overall, these findings underscore the nuanced interplay between shape parameters, node density, time step size, and method selection in determining the accuracy and efficiency of meshless methodologies in various simulation contexts.

REFERENCES

[1] Zeidan D, Romenski E, Slaouti A, Toro EF. Numerical study of wave propagation in compressible two-phase flow, International journal for numerical methods in fluids, 2007, 54(4), 393-417. DOI:https://doi.org/10.1002/fld.1404

[2] Zeidan D, Assessment of mixture two-phase flow equations for volcanic flows using Godunov-type methods, Applied Mathematics and Computation, 2016, 272, 707-19. DOI: https://doi.org/10.1016/j.amc.2015.09.038

[3] Goncalvès E, Zeidan D, Numerical simulation of unsteady cavitation in liquid hydrogen flows, International Journal of Engineering Systems Modelling and Simulation, 2017, 9(1), 41-52. DOI: https://doi.org/10.1504/IJESMS.2017.081736

[4] Zeidan D, Sekhar TR, On the wave interactions in the drift-flux equations of two-phase flows, Applied Mathematics and Computation, 2018, 327, 117-31. DOI: https://doi.org/10.1016/j.amc.2018.01.021

[5] Agbavon KM, Appadu AR, Khumalo M, On the numerical solution of Fisher's equation with coefficient of diffusion term much smaller than coefficient of reaction term, Advances in Difference Equations, 2019, 2019(1), 1-33. DOI: https://doi.org/10.1186/s13662-019-2080-x

[6] Young DL, Chen CH, Fan CM, Shen LH, The method of fundamental solutions with eigenfunctions expansion method for 3D nonhomogeneous diffusion equations, Numerical Methods for Partial Differential Equations: An International Journal, 2009, 25(1), 195-211. DOI: https://doi.org/10.1002/num.20336.

[7] Wang F, Chen W, Tadeu A, Correia CG, Singular boundary method for transient convection–diffusion problems with time-dependent fundamental solution, International Journal of Heat and Mass Transfer, 2017, 114, 1126-34. DOI: https://doi.org/10.1016/j.ijheatmasstransfer.2017.07.007.

[8] Lin J, Reutskiy SY, Lu J, A novel meshless method for fully nonlinear advection–diffusion-reaction problems to model transfer in anisotropic media, Applied Mathematics and Computation, 2018, 339, 459-76. DOI:https://doi.org/10.1016/j.amc.2018.07.045.

[9] Fu ZJ, Xi Q, Chen W, Cheng AH, A boundary-type meshless solver for transient heat conduction analysis of slender functionally graded materials with exponential variations, Computers & Mathematics with Applications, 2018, 76(4), 760-73. DOI: https://doi.org/10.1016/j.camwa.2018.05.017

[10] Zhou ZJ, Yan NN, A survey of numerical methods for convection–diffusion optimal control problems, Journal of Numerical Mathematics, 2014, 22(1), 61-85. DOI: https://doi.org/10.1515/jnum-2014-0003

[11] Chen BM, Kojouharov HV, Non-standard numerical methods applied to subsurface biobarrier formation models in porous media, Bulletin of mathematical biology, 1999, 61(4), 779-98. DOI: https://doi.org/10.1006/bulm.1999.0113

[12] Sengupta S, Sreejith NA, Mohanamuraly P, Staffelbach G, Gicquel L, Global spectral analysis of the Lax–Wendroff-central difference scheme applied to Convection–Diffusion equation, Computers & Fluids, 2022, 242, 105508. DOI:

https://doi.org/10.1016/j.compfluid.2022.105508

[13] Wang X, Malluwawadu NS, Gao F, McMillan TC, A modified weak Galerkin finite element method, Journal of Computational and Applied Mathematics, 2014, 271, 319-27. DOI:https://doi.org/10.1016/j.cam.2014.04.014

[14] Fallahzadeh A, Shakibi K, A method to solve Convection-Diffusion equation based on homotropy analysis method, Journal of interpolation and approximation in scientific computing, 2015, 2015(1), 1-8. DOI: https://doi.org/10.5899/2015/jiasc-00074

[15] Safdari-Vaighani A, Heryudono A, Larsson E, A radial basis function partition of unity collocation method for convection–diffusion equations arising in financial applications, Journal of Scientific Computing, 2015, 64(2), 341-67. DOI: https://doi.org/10.1007/s10915-014-9935-9

[16] Qian L, Feng X, He Y, The characteristic finite difference streamline diffusion method for convection-dominated diffusion problems, Applied Mathematical Modelling, 2012, 36(2), 561-72. DOI:https://doi.org/10.1016/j.apm.2011.07.034

[17] Zhai S, Qian L, Gui D, Feng X, A block-centered characteristic finite difference method for convection-dominated diffusion equation, International Communications in Heat and Mass Transfer, 2015, 61, 1-7. DOI: https://doi.org/10.1016/j.icheatmasstransfer.2014.11.003.

[18] Funaro D, A new scheme for the approximation of advection-diffusion equations by Collocation, SIAM journal on numerical analysis, 1993, 30(6), 1664-76. DOI: https://doi.org/10.1137/0730085.

[19] Si Z, Feng X, Abduwali A, The semi-discrete streamline diffusion finite element method for time-dependented convection–diffusion problems, Applied Mathematics and Computation, 2008, 202(2), 771-9. DOI: https://doi.org/10.1016/j.amc.2008.03.021.

[20] Rui H, Tabata M, A second order characteristic finite element scheme for convection-diffusion problems, Numerische Mathematik, 2002, 92(1), 161-77. DOI: https://doi.org/10.1007/s002110100364

[21] Chen C, Bi C, Two-grid methods for characteristic finite volume element solution of semilinear convection–diffusion equations, Applied Mathematics and Computation, 2010, 217(5),1896-906. DOI:https://doi.org/10.1016/j.amc.2010.06.044

[22] Wang S, Solving convection-dominated anisotropic diffusion equations by an exponentially fitted finite volume method, Computers & Mathematics with Applications. 2002, 44(8-9), 1249-65. DOI: https://doi.org/10.1016/S0898-1221(02)00230-4

[23] Tan J, An upwind finite volume method for convection-diffusion equations on rectangular mesh, Chaos, Solitons & Fractals, 2019, 118, 159-65. DOI: https://doi.org/10.1016/j.chaos.2018.09.011

[24] Russo A, Streamline-upwind Petrov/Galerkin method (SUPG) vs residual-free bubbles (RFB), Computer methods in applied mechanics and engineering, 2006, 195(13-16), 1608-20. DOI:https://doi.org/10.1016/j.cma.2005.05.031

[25] Knobloch P, A generalization of the local projection stabilization for convection-diffusion-reaction equations, SIAM journal on numerical analysis, 2010, 48(2), 659-80. DOI:https://doi.org/10.1137/090767807

[26] Zhang SH, Wang WQ, A stencil of the finite-difference method for the 2D convection diffusion equation and its new iterative scheme, International Journal of Computer Mathematics, 2010, 87(11), 2588-600. DOI: https://doi.org/10.1080/00207160802691637

[27] Falini A, Sampoli ML, Adaptive Refinement in Advection–Diffusion Problems by Anomaly Detection: A Numerical Study, Algorithms, 2021, 14(11), 328. DOI: https://doi.org/10.3390/a14110328

[28] Partridge PW, Brebbia CA, editors. Dual reciprocity boundary element method. Springer Science & Business Media; 2012 Dec 6.

[29] Chanthawara K, Kaennakham S, Toutip W, The numerical study and comparison of radial basis functions in applications of the dual reciprocity boundary element method to convection-diffusion problems, InAIP Conference Proceedings, 2016, 1705(1). AIP Publishing. DOI: https://doi.org/10.1063/1.4940277.

[30] Bokota A, Iskierka S, An analysis of the diffusion-convection problem by the boundary element method, Engineering analysis with boundary elements, 1995, 15(3), 267-75. DOI: https://doi.org/10.1016/0955-7997(95)00031-I

[31] W. Toutip, The dual reciprocity boundary element method for linear and nonlinear, Ph. D Thesis (University of Hertfordshire, United Kingdom, 2001).

[32] Zheng H, Zhang C, Wang Y, Sladek J, Sladek V, A meshfree local RBF collocation method for anti-plane transverse elastic wave propagation analysis in 2D phononic crystals, Journal of Computational Physics, 2016, 305, 997-1014. DOI: https://doi.org/10.1016/j.jcp.2015.10.020

[33] Li N, Tan Z, Feng X, Novel two-level discretization method for high dimensional semilinear elliptic problems base on RBF-FD scheme, Numerical Heat Transfer, Part B: Fundamentals, 2017, 72(5), 349-60. DOI: https://doi.org/10.1080/10407790.2017.1409511

[34] Qiao Y, Zhai S, Feng X, RBF-FD method for the high dimensional time fractional convection-diffusion equation, International Communications in Heat and Mass Transfer, 2017, 89, 230-40. DOI: https://doi.org/10.1016/j.icheatmasstransfer.2017.08.016

[35] Oñate E, Idelsohn S, Zienkiewicz OC, Taylor R, A finite point method in computational mechanics Applications to convective transport and fluid flow, International journal for numerical methods in engineering, 1996, 39(22), 3839-66. DOI: https://doi.org/10.1002/(SICI)1097-0207(19961130)39:22<3839::AID-NME27>3.0.CO;2-R.

[36] Liszka TJ, Duarte CA, Tworzydlo W, hp-Meshless cloud method, Computer Methods in Applied Mechanics and Engineering, 1996, 139(1-4), 263-88. DOI: https://doi.org/10.1016/S0045-7825(96)01086-9

[37] Hu DA, Long SY, Liu KY, Li GY, A modified meshless local Petrov–Galerkin method to elasticity problems in computer modelling and simulation, Engineering analysis with boundary elements. 2006, 30(5), 399-404. DOI: https://doi.org/10.1016/j.enganabound.2005.12.002

[38] Nayroles B, Touzot G, Villon P, Generalizing the finite element method: diffuse approximation and diffuse elements, Computational mechanics, 1992, 10(5), 307-18. DOI:https://doi.org/10.1007/BF00364252

[39] Liu GR, Gu Y, A point interpolation method for two-dimensional solids, International journal for numerical methods in engineering, 2001, 50(4), 937-51. DOI: https://doi.org/10.1002/1097-0207(20010210)50:4<937::AID-NME62>3.0.CO;2-X

[40] Kansa EJ, Multiquadrics—A scattered data approximation scheme with applications to computational fluid-dynamics—II solutions to parabolic, hyperbolic and elliptic partial differential equations, Computers & mathematics with applications, 1990, 19(8-9), 147-61. DOI: https://doi.org/10.1016/0898-1221(90)90271-K

[41] Sharan M, Kansa EJ, Gupta S, Application of the multiquadric method for numerical solution of elliptic partial differential equations, Applied Mathematics and Computation, 1997, 84(2-3), 275-302. DOI: https://doi.org/10.1016/S0096-3003(96)00109-9

[42] Pang G, Chen W, Fu Z, Space-fractional advection–dispersion equations by the Kansa method, Journal of Computational Physics, 2015, 293, 280-96. DOI: https://doi.org/10.1016/j.jcp.2014.07.020

[43] Sarra SA, Cogar S, An examination of evaluation algorithms for the RBF method, Engineering Analysis with Boundary Elements, 2017, 75, 36-45. DOI: https://doi.org/10.1016/j.enganabound.2016.11.006

[44] Fallah A, Jabbari E, Babaee R, Development of the Kansa method for solving seepage problems using a new algorithm for the shape parameter optimization, Computers & Mathematics with Applications, 2019, 77(3), 815-29. DOI: https://doi.org/10.1016/j.camwa.2018.10.021

[45] Chen W, Hong Y, Lin J, The sample solution approach for determination of the optimal shape parameter in the Multiquadric function of the Kansa method, Computers & Mathematics with Applications, 2018, 75(8), 2942-54. DOI: https://doi.org/10.1016/j.camwa.2018.01.023

[46] Haq S, Hussain M, The meshless Kansa method for time-fractional higher order partial differential equations with constant and variable coefficients, Revista de la Real Academia de Ciencias Exactas, Físicas y Naturales. Serie A. Matemáticas, 2019, 113(3), 1935-54. DOI:https://doi.org/10.1007/s13398-018-0593-x

[47] Verma R, Kumar S, Computational study on constant and sinusoidal heating of skin tissue using radial basis functions, Computers in Biology and Medicine, 2020, 121, 103808. DOI:https://doi.org/10.1016/j.compbiomed.2020.103808

[48] Li J, Zhai S, Weng Z, Feng X, H-adaptive RBF-FD method for the high-dimensional convection-diffusion equation, International Communications in Heat and Mass Transfer, 2017, 89, 139-46. DOI: https://doi.org/10.1016/j.icheatmasstransfer.2017.06.001

[49] Li N, Su H, Gui D, Feng X, Multiquadric RBF-FD method for the convection-dominated diffusion problems base on Shishkin nodes, International Journal of Heat and Mass Transfer, 2018, 118, 734-45. DOI: https://doi.org/10.1016/j.ijheatmasstransfer.2017.11.011

[50] Chuathong N, Kaennakham S, A numerical investigation on variable shape parameter schemes in a meshfree method applied to a convection-diffusion problem, International Journal of Applied Engineering Research, 2017, 12(14), 4162-70. DOI: https://www.ripublication.com/ijaer17/ijaerv12n14_16.pdf

[51] Chuathong N, Kaennakham S, Toutip W, An automatic centroid-node adaptive meshless (CNAM) method for solving convection-diffusion problems, Journal of Engineering and Applied Science, 2017, 12, 6554-291. DOI: http://dx.doi.org/10.36478/jeasci.2017.6884.6891

[52] Kaennakham S, Chuathong N, An automatic node-adaptive scheme applied with a RBF-collocation meshless method, Applied Mathematics and Computation, 2019, 348, 102-25. DOI:https://doi.org/10.1016/j.amc.2018.11.066

[53] Chanthawara K, Kaennakham S, Modelling Steady Convection-Dominated Phenomena by Node-Adaptive Radial Point Interpolation Meshfree Method (RPIM) with Various RBFs, InJournal of Physics: Conference Series, 2020, 1489(1), 012011. IOP Publishing. DOI: https://iopscience.iop.org/article/10.1088/1742-6596/1489/1/012011.

[54] Kaennakham S, Chuathong N, Numerical simulation of convection-diffusion phenomena by four inverse-quadratic-RBF domain-meshfree schemes, The International Journal of Multiphysics, 2019, 13(1), 1-30. DOI: https://doi.org/10.21152/1750-9548.13.1.1

[55] Bellman R, Kashef BG, Casti J, Differential quadrature: a technique for the rapid solution of nonlinear partial differential equations, Journal of computational physics, 1972, 10(1), 40-52. DOI:https://doi.org/10.1016/0021-9991(72)90089-7

[56] Wu YL, Shu C, Development of RBF-DQ method for derivative approximation and its application to simulate natural convection in concentric annuli, Computational Mechanics, 2002, 29, 477-85. DOI:https://doi.org/10.1007/s00466-002-0357-4

[57] Chen CS, Jankowska MA, Karageorghis A, RBF–DQ algorithms for elliptic problems in axisymmetric domains, Numerical Algorithms, 2022, 89, 33-63. DOI: https://doi.org/10.1007/s11075-021-01105-w

[58] Motaman F, Rakhshandehroo GR, Hashemi MR, Niazkar M, Application of RBF-DQ method to time-dependent analysis of unsaturated seepage, Transport in Porous Media, 2018, 125, 543-64. DOI:https://doi.org/10.1007/s11242-018-1138-7

[59] Parand K, Hashemi S, RBF-DQ method for solving non-linear differential equations of Lane-Emden type, Ain Shams Engineering Journal, 2018, 9(4), 615-29. DOI: https://doi.org/10.1016/j.asej.2016.03.010

[60] Mai-Duy N, Tran-Cong T, An efficient indirect RBFN-based method for numerical solution of PDEs, Numerical Methods for Partial Differential Equations: An International Journal, 2005, 21(4), 770-90. DOI: https://doi.org/10.1002/num.20062

[61] Sarra SA, Integrated multiquadric radial basis function approximation methods, Computers & Mathematics with Applications, 2006, 51(8), 1283-96. DOI: https://doi.org/10.1016/j.camwa.2006.04.014

[62] Tien CM, Thai-Quang N, Mai-Duy N, Tran CD, Tran-Cong T, A three-point coupled compact integrated RBF scheme for second-order differential problems, CMES: Computer Modelling in Engineering & Sciences, 2015, 104(6), 425-69. DOI: https://doi.org/10.3970/cmes.2015.104.425

[63] Shu C, Wu YL, Integrated radial basis functions-based differential quadrature method and its performance, International Journal for Numerical Methods in Fluids, 2007, 53(6), 969-84. DOI: https://doi.org/10.1002/fld.1315

[64] Ebrahimijahan A, Dehghan M, Abbaszadeh M, Numerical simulation of shallow water waves based on generalized equal width (GEW) equation by compact local integrated radial basis function method combined with adaptive residual subsampling technique, Nonlinear Dynamics, 2021, 105(4), 3359-91. DOI: https://doi.org/10.1007/s11071-021-06733-4

[65] Mai-Duy N, Tran-Cong T, Approximation of function and its derivatives using radial basis function networks, Applied Mathematical Modelling, 2003, 27(3), 197-220. DOI: doi:10.1016/s0307-904x(02)00101-4.

[66] Yao G, Šarler B, Chen CS, A comparison of three explicit local meshless methods using radial basis functions, Engineering Analysis with Boundary Elements, 2011, 35(3), 600-9. DOI:http://dx.doi.org/10.1016/j.enganabound.2010.06.022

[67] Carlsow HS, Jaeger JC. Condution of heat in solids.

[68] Sun HW, Li LZ, A CCD–ADI method for unsteady convection–diffusion equations, Computer Physics Communications, 2014, 185(3), 790-7. DOI: http://dx.doi.org/10.1016/j.cpc.2013.11.009

[69] Boztosun I, Charafi A, An analysis of the linear advection–diffusion equation using mesh-free and mesh-dependent methods, Engineering Analysis with Boundary Elements, 2002, 26(10), 889-95. DOI: https://doi.org/10.1016/S0955-7997(02)00053-X.